Systematic search for repeating earthquakes along the Haiyuan fault system in Northeastern Tibet

Yangfan Deng[1,2], Zhigang Peng[2], Jing Liu-Zeng[3]

[1] *State Key Laboratory of Isotope Geochemistry, Guangzhou Institute of Geochemistry, Chinese Academy of Sciences, Guangzhou, 510640, China*

[2] *School of Earth and Atmospheric Sciences, Georgia Institute of Technology, Atlanta, GA, 30332, USA*

[3] *Institute of Surface-Earth System Science, Tianjin University, Tianjin, 300072, China*

Correspondence to: Y. Deng and Z. Peng, yangfandeng@gig.ac.cn; zpeng@gatech.edu

Abstract: Repeating earthquakes have been found at many faults around the world, and they provide valuable information on diverse faulting behavior at seismogenic depth. The Haiyuan fault is a major left-lateral strike-slip fault along the northeastern (NE) boundary of the Tibetan Plateau. Two great earthquakes (1920 Haiyuan, 1927 Gulang) have occurred on this fault system, but the section between the ruptures of the two earthquakes, also known as the Tianzhu seismic gap, remains unbroken. Shallow creep has been observed from geodetic data at the eastern end of the seismic gap. However, the driving mechanism and depth extent of shallow creep are not clear. Here we conduct a systematic search for repeating earthquakes in NE Tibet based on seismic data recorded by permanent stations in ten years (2009-2018). Based on waveform cross-correlations and subsequent relocations, we find several repeating earthquake clusters at the Laohushan section. This is consistent with the shallow creep inferred from the geodetic data, indicating repeating earthquakes can be driven by nearby aseismic slip. ~300 repeaters were found within clusters of intense seismicity near the rupture zones of the 1927 M8.0 Gulang and 2016 M6.4 Menyuan

earthquakes. Relocation of events in the cluster near the Gulang earthquake delineates two possible unmapped faults orthogonal to the Haiyuan fault. In addition, we also identify several repeating earthquakes generated by mining activities with different waveforms and occurrence patterns. Our study suggests that repeating earthquakes around the Haiyuan fault are mostly driven by postseismic relaxation process associated with the 1920 Haiyuan and 1927 Gulang earthquakes.

Plain Language Summary: Repeating earthquakes usually have a similar magnitude and occur at the same fault patch. Based on the ten years data in NE Tibet, we find ~10 % of events in NE Tibet are repeating events. The repeating earthquakes at Laohushan section of Haiyuan fault mark the boundary between the creep and locked region. The repeating earthquakes at Menyuan follow the moderate-size mainshocks. The intense seismicity at the Gulang seismic zone reveals two possible hidden faults. Mining related repeaters have different waveforms from natural earthquakes and occur dominantly in afternoons, inferring that repeaters along the Haiyuan fault are of earthquake origin and indicators of faulting behavior.

Key points:

1. Repeating earthquakes are found at the creeping Laohushan section of the Haiyuan Fault.
2. Intense seismicity at the Gulang seismic zone reveals two possible hidden faults.
3. Repeating earthquakes along the Haiyuan Fault are likely driven by postseismic processes of large earthquakes.

Introduction

Repeating earthquakes (also known as repeaters) are families of seismic events generated by repeated loading and failure of a single fault patch (e.g., Vidale et al., 1994; Nadeau et al., 1995). Because they are typically driven by aseismic slow slip surrounding them (Beeler et al., 2001), repeaters provide new insight into diverse fault slip behavior at depth, which is usually difficult to characterize from surface observations alone. These include postseismic afterslip, triggered creep and eposodic slow slip events, and steady fault creep during interseismic period (Uchida and Bürgmann, 2019; Uchida, 2019). In addition, repeating earthquakes can be used to quantify temporal changes of seismic velocities (e.g., Poupinet et al., 1984; Schaff and Beroza, 2004; Rubinstein and Beroza, 2004; Peng and Ben-Zion, 2006) or seismic scatterers at depth (Niu et al., 2003; Taira et al., 2009).

Repeating earthquakes was first identified in Central California along the Calaveras Fault (Vidale et al., 1994) and the Parkfiled section of the San Andreas Fault (Nadeau et al., 1995). Since then, they have been found on major plate boundary faults elsewhere around the world, such as the Japan trench (e.g. Igarashi et al., 2003; Uchida et al., 2003), Taiwan (Chen et al., 2007), Tonga (eg. Yu, 2013), Costa Rica (Yao et al., 2017), and Turkey (Peng and Ben-Zion, 2005, 2006). There are also increasing reports on repeating earthquakes in intraplate settings. For example, repeaters have been found in seismic zones in the central United States (Bisrat et al. 2012). Based on cross-correlating of regional seismic waveforms, Schaff and

75 Richards (2004) found that 10% of seismic events in and around China are repeating
76 earthquakes (with no more than 1 km from each other). In addition, Li et al. (2007)
77 found repeaters in eastern China along the aftershock zone of the 1976 M7.6
78 Tangshan earthquake, and Li et al. (2011) identified repeaters in the Longmen Shan
79 Thrust Fault zone along the rupture zone of the 2008 Mw7.9 Wenchuan earthquake.
80 Liu et al. (2019) found the repeating earthquake clusters in the aftershock zone of the
81 2016 Ms6.4 Menyuan earthquake along the northeastern (NE) margin of the Tibetan
82 Plateau.

83 The Haiyuan fault (HYF) is a major active left-lateral strike-slip fault along the
84 NE edge of the Tibetan Plateau (Figure 1). The western and central sections include
85 the Lenglengling fault (LLLF), Jinqianghe fault (JQHF), Maomaoshan fault (MMSF),
86 Laohushan fault (LHSF), and the eastern section connects with the Liupanshan fault
87 (LPSF) at Madongshan (MDS). Several large earthquakes occurred along the Haiyuan
88 fault system in the past, including the 1920 M7.8-8.3 Haiyuan (Liu-Zeng et al., 2015),
89 the 1927 M~8 Gulang, the 1990 Ms6.2 Jingtai and the 2016 Ms6.4 Mengyuan
90 earthquakes. However, there is not yet the consensus of the slip rate along the HYF.
91 Based on the ages of fault-related, scarp-derived colluvial wedges, Zhang et al. (1998)
92 obtained a slip rate of 8 ± 2 mm/yr along the eastern section of the HYF. Based on
93 offset geomorphic features and age constraints, Li et al. (2009) inferred a slip rate of
94 4.5 ± 1.0 mm/yr on the same section. However, Lasserre et al. (1999) yielded a high
95 slip rate (12 ± 4 mm/yr) in the middle section, which was recently re-evaluated and

updated to be 5-9 mm/yr (Yao et al., 2019).

At the east end of the middle Laohushan section, shallow creep has been observed from geodetic data and is estimated to be 5 ± 1 mm/yr (Jolivet et al., 2012, 2013), close to or slightly smaller than the geologic rate. However, creep in this section is poorly understood as compared to other known creeping faults of fault sections around the world (e.g., Harris, 2017). For example, the depth extent of the creep is not well constrained. In addition, it is unclear whether creep on this section of the HYF is a transient phenomenon following the 1920 Haiyuan mainshock, or reflects a long-term slip behavior (Chen et al., 2018).

In order to better understand the seismicity pattern and fault slip behaviors along the HYF, we conduct a systematic search for repeating earthquakes in this region based on ten years of microseismic data. Specifically, we identify repeating earthquake pairs using waveform cross-correlations, and then we group the pair into clusters. Finally, we use these repeating clusters to better understand the aseismic process and slip rates along the HYF and other faults in NE Tibet.

Data and Methods

Within the following geographic boundaries (longitudes between 96-107°E, latitudes between 36-41°N), there are more than 25,000 M≥1 events from 2009 to 2018 based on the regional catalog archived by the China Earthquake Networks Center (CENC) (Figure 1). The earthquakes are mostly distributed along the HYF and other major faults/boundaries in this region, such as near the eastern end of the ATF,

and the western boundary of the Ordos basin. We obtain raw seismogram data (100 Hz sampling rate) recorded by 51 permanent stations from the Data Management Centre of the China National Seismic Network (Zheng et al. 2010). These include 44 stations deployed before 2009, and 7 stations deployed at the end of 2014 (Figure S1).

Hypocenter location and waveform similarity are two main methods to identify repeating earthquakes (Uchida, 2019). Here we use the later one because it is the most frequently used method and we can relocate the events afterwards. Our analysis procedure includes the following six steps. First, we compute the P and S arrival time using the Taup program (Crotwell et al., 1999) according to a local velocity model (Deng et al., 2018; Table S1) modified from isap91 model (Kennett and Engdahl, 1991). Because there are some hand-picked P and S phases in the catalog, we use them when available, and use the computed arrival times for the rest traces. We then apply a 2-16 Hz bandpass filter on the data, which is the predominant frequency range for microearthquakes (Uchida, 2019). Next, we perform a quality control on the raw data, based on the signal-noise-ratio (SNR). We use a 20-s window (5 s before the P wave) as the signal window, and the same 20-s window 25 s before the P wave as the noise window. We choose the data with the SNR higher than 4 and remove the rest seismograms with low SNRs.

We then compute cross-correlations (CCs) among all M≥1 events beneath all stations, and identify repeating event pairs with locations less than 200 km apart with CC value above 0.80. Because the time windows are usually set to contain both P and

S phases to ensure the same P-S time and thus the same hypocentral distance (Uchida et al., 2003), here we choose 2 s before and 18 s after the P arrivals. The predicted P arrival may be not accurate due to the complicated velocity structure and inaccurate epicentral location, so we allow a maximum time shift of 5 s to obtain the highest CC between each waveform pair. Next, we group repeating pairs into clusters using an Equivalency Class (EC) algorithm (Peng and Ben-Zion, 2005; Press et al., 1986). When two pairs have a common event and meet a certain threshold (median CC value ≥ 0.9 with number of at least 2 stations), we group them into the same cluster. Finally, we relocate the repeaters in each cluster using the Growclust program (Trugman et al., 2017) based on the differential arrival times from waveform cross-correlations.

Based on the identified repeaters, we can estimate their cumulative slip according to their local magnitudes M_L. The individual slip d can be estimated by assuming a standard crack model

$$d = \frac{M_0}{\mu \pi r^2} \quad (1)$$

where r is the rupture size, and M_o is the seismic moment. The rupture size r can be obtained from (Kanamori and Anderson, 1975)

$$r = \left(\frac{7M_0}{16\Delta\sigma}\right)^{1/3} \quad (2)$$

where $\Delta\sigma$ is the static stress drop. The seismic moment M_o can be estimated from the local magnitude M_L with the following equation (Abercrombie, 1996)

$$\log(M_0) = 9.8 + M_L \quad (3)$$

Finally, the average slip rate is computed from dividing the cumulative slip with

160 the total duration of the repeating cluster (Li et al., 2011).

161 While the local magnitudes M_L can be obtained from the CENC catalog, the
162 stress drops $\Delta\sigma$ for these events are not available. Hence, we use nominal stress drop
163 values of 1, 5 and 10 MPa, respectively (Li et al., 2011).

164

165 **Results**

166 In total, we identify 929 clusters (~2,500 events) in NE Tibet with at least two
167 repeaters, which accounts for ~10% of earthquakes in this region. Figure 2 shows the
168 spatial distribution of all repeating clusters, together with the background seismicity.
169 Even though the repeaters are widely distributed, clusters with more than 8 events are
170 only found at certain regions along and outside of the HYF. In the following sections,
171 we discuss them in more detail.

172 ***1) The creeping section of the HYF (middle Laohushan section) (region 1)***

173 We find the 31 repeating earthquakes within 12 clusters along the LHSF, which is
174 in the central section of the HYF (Figure 3). From the map view, the repeaters are
175 mostly located around 103.7°E, to the west side of the peak creep region as reported
176 by Jolivet et al. (2013). 87 % and 94 % repeaters have the depth shallower than 10 km
177 before and after relocation, respectively. Figure 4 shows an example of waveforms
178 recorded at station GS.JDT for the repeating earthquake cluster with 8 events, which
179 occurred from 2013 to 2017. The waveforms show high similarity from the P and S
180 waves to the coda waves, and their magnitudes are similar, indicating that they likely

rupture the same fault patch at depth.

Between the analyzed time period (2009-2019), a total of four events with moment magnitude Mw≥4 occurred in this region, and two of them have focal mechanisms estimated with the gCAP method (Cui et al., 2019). If we include three more events listed in the global CMT (GCMT) catalog, four of them have strike-slip focal mechniams and the other one (2009 M4.3) is a thrust event. We observe an increasing occurrence of repeating events (as well as background events) following the 2014/11/14 M4.9 and 2015/07/15 M4.0 strike-slip events. No obvious change in repeating earthquake (and background event) was found following the 2009/10/27 M4.3 thrust and 2018/05/26 M4.1 event (focal mechanisms not determined).

Table S2 summarizes the estimated slip rates for 6 repeating clusters along the LHSF with three nominal stress drop values. For the cluster with number of events, the corresponding slip rates with 1, 5 and 10 MPas stress drops are 0.77, 2.25, and 3.58 mm/yr, respectively. If we take the results with 5 MPa for later comparison with results along the Wenchuan aftershock zone by Li et al. (2011), the average slip rate of these repeating earthquakes is 2.25 ± 2.24 mm/yr.

2) Aftershock zone of the 2016 Menyuan earthquake (region 2)

A strong earthquake with a magnitude of Ms6.4 occurred at Menyuan, Qinghai Province of China at 2016/01/21, close to the LLLF at the western edge of the HYF. In addition to this event, several moderate-size earthquakes, such as the 1986 M5.4,

1987 M6.5, 1991 M5.2, and 2013 M5.3 earthquakes, also occurred in this region (Li et al., 2016). Based on the matched filter detection and relocation of early aftershocks, Liu et al. (2019) inferred that the 2016 Mengyuan mainshock occurred on a steeply dipping secondary fault rather than the major LLLF. This interpretation is consistent with the geodetic and geological observations (Li et al., 2016). Liu et al., (2019) also found 26 repeating clusters (~172 events) in the aftershock zone of the Mengyuan mainshock.

From ten years of seismic data, we identify 81 events within 37 clusters in this region (Figure 5). Most of them occurred following the 2016 Ms6.4 mainshock. A subtle increase of repeating events is also observed after the 2016 M4.7 and 2017 M4.1 events (likely aftershocks of the Ms6.4 mainshock), but not following the 2013 M5.3 event. Because repeating aftershocks are mostly driven by afterslip (Schaff and Beroza, 2004; Peng et al. 2005), their recurrence times increase following the Mengyuan mainshock (Liu et al. 2019). Hence we do not compute their cumulative slip and average slip rate in this region.

3) Gulang seismic zone, north of the HYF (region 3)

We found 210 repeating earthquakes (75 clusters) that occurred in the Gulang seismic zone near the epicenter of the 1927 Gulang earthquake (Figure 6). From the map view, these repeating earthquakes are located between the strike-slip HYF in the south and the south-dipping Huangcheng-Shuangta fault (HC-STF) in the north. The

223 repeating earthquakes are within the clusters of intensive background seismicity that
224 deneate two nearly N-S striking features. But there are no mapped faults on the
225 surface. These repeating earthquakes occurred every year from 2009 to 2018. We find
226 that repeating earthquake rates increased after the 2011/02/22 M4.1 event, 2014/02/22
227 M 4.5 event and 2014/03/12 M 4.1 event. In comparison, some repeating clusters are
228 not related with any moderate-size earthquakes. For example, 10 repeating
229 earthquakes occurred in a tight cluster between 2013/07/03 and 2013/07/04 with very
230 short occurrence intervals (marked as C3 in Figure 6). Similar repeating clusters occur
231 on 2009/06/21 (C1), 2012/06/24 (C2), and 2017/06/08 (C4). Since these sequences do
232 not have a clear moderate-size mainshock (earthquakes with M≥4, Figure 6), they
233 may be considered as earthquake swarms (Vidale and Shearer, 2006).
234
235 4) Mining related repeaters
236 In the CENC catalog, there are 332 marked mining explosions at the boundary
237 between Neimenggu and Ningxia Provinces (39.0-39.2°N, 105.95-106.15°E. Marked
238 as region 5 in Figure 2). Because mining explosions almost occur in the same position,
239 the corresponding seismic waveforms have very high similarities and can be detected
240 as repeaters in this study. In our study region we find 136 possible repeating events
241 within 25 clusters that are likely mining related.
242 We use the following evidence to confirm these events are likely related to
243 mining activities. First, some events listed in the repeating clusters are marked as

mining explosion in the CENC catalog. Second, the local times of these events have peaks in the afternoon instead of a uniform distribution (Figure 7), which is consistent with the expected mining explosion schedule (e.g., Ruan et al., 2017). Third, we can identify possible mining related images with Google Map in this region (Figure 8). Finally, the event magnitudes are tightly clustered (Figure 9), and there are no M>4 events in this region.

In addition to this region, we also find three other regions (regions 6-8 in Figure 2) with possible mining explosions. Compared with clear P and S arrivals for regular earthquakes, explosion-generated waveforms have different phases (Figures 3 and 9). We note that the first few cycles of the P waves are not quite the same among these regions (Figure 9), which may indicate different styles of explosions (e.g., delayed versus single fire) (Stump et al., 2002), as well as possible structural difference.

There are also some repeating events in other places, such as MDS that is marked as region 4 in Figure 2. If there are no M>4 events and no marked surface fault, we generally consider them as possible mining explosions.

Discussion

1. The characteristics of repeating earthquakes at LHSF

In this study, we identified 12 clusters with 31 repeating events along and near the Laohushan section of the HYF, where surface creep has been identified (Jolivet et al., 2013). As mentioned before, it is still not clear what is the cause of creep in this

region. There is some evidence for the surface-breaking rupture of paleo-earthquakes in this section. In addition, the cumulative slip offset in this region is similar to non-creeping brittle faults (Chen et al., 2018). Based on these observations, Chen et al. (2018) inferred that either the fault is capable of switching between creeping and brittle faulting over time, or the fault is partially creeping, capable of both creeping and surface-rupturing brittle faulting. In the second possibility, the creep on the Laohushan section is a shallow phenomenon, with the fault remaining locked at depth, similar to the Ismetpasa segment of the North Anatolian fault in Turkey (Ozener et al., 2010; Karabacak et al., 2011; Kaneko et al., 2013) and the Hayward fault in northern California (Simpson et al., 2001; Schmidt et al., 2005).

Based on an assumed stress drop of 1, 5 and 10 MPas (Li et al., 2011), we computed the cumulative slip and slip rate of the repeating earthquakes in this region. We found that the largest slip rate is 6.6 mm/yr and the average slip rate is 2.25 ± 2.24 mm/yr. Although with large uncertainties, our estimated slip rate is less than the shallow creep rate of ~5 mm/yr from InSAR observations (Jolivet et al., 2013) and geological rate of 5-9 mm/yr (Yao et al., 2019).

Our estimation of slip rate based on repeating clusters has several limitations. First, we only take the M≥1 events into account. Hence, seismic slip released by events with smaller magnitudes is not included. Second, the M≥1 events catalog may be incomplete, which could result in a biased estimation of slip rate. Finally, it is possible that some asperities creep at interseismic time periods (Beeler et al., 2001).

Hence, what we estimate here can be considered as the lower bound of the actual slip rate, although we do not expect to observe several folds increase in the slip rate.

After the relocation, the repeaters are mostly located between 4-8 km depth (Figure 10), which is below the inferred depth of shallow creep (Jolivet et al. 2013). In addition, these repeaters occurred to the west of the peak creep observed from InSAR observation (Jolivet et al. 2013). Our observation suggests that the geodetically observed creep is constrained at shallow depth, while faults at deeper depth remain locked. Hence, these repeating earthquakes likely marked the boundary between the creep and locked region, similar to the Parkfield section of the San Anderas Fault (Nadeau and McEvilly, 1999, 2004; Lengline and Marsan, 2009), the Morgan Hill section of the Calaveras Fault (Rubin, 2002; Schaff et al., 2002; Peng et al., 2005), as well as the Hayward Fault (Bürgmann et al., 2000; Shirzaei et al., 2013). This is also compatible with the observation of earthquake swarms driven by shallow aseismic slip in Salton Trough, California (Lohman and McGuire, 2007), and anticorrections between afterslip and aftershocks (including repeating earthquakes) following the 2012 M7.6 Nicoya, Costa Rica, earthquake (Hobbs et al., 2017; Yao et al., 2017). These studies suggest that while microseismicity (including earthquake swarms and repeating earthquakes) can be driven by nearby aseismic slip, they likely occur in slightly different regions, indicating varying frictional behavior along dip and strike directions.

Considering that the creeping Laohushan section on the HYF is located

immediately to the west of 230-km surface rupture of the 1920 Haiyuan M7.8 earthquake, Chen et al. (2018) speculated that long-term post-seismic deformation following the 1920 Haiyuan mainshock might have a heightened effect on creep rate observed recently. The creeping section is also located at the eastern end of the over-200 km long “quite” seismic gap, known as the Tianzhu gap (Gaudemer *et al.*, 1995). Hence, the Laohushan section is somewhat similar to the creeping section of the San Andreas Fault from Parkfield to Hollister in Central California, which was sandwiched between the 1857 Fort Tejon and 1906 San Francisco earthquakes. However, the creeping section of the Haiyuan fault is only 35 km (Jolivet et al. 2012), much shorter than the ~150 km length for the San Andreas Fault. While the creeping section is generally considered as ‘barrier’ to seismic ruptures, Noda and Lapusta (2013) demonstrated that dynamic earthquake ruptures (combined with co-seismic weakening) can break through long portions of creeping faults, indicating the possibility a total rupture on long strike-slip faults such as the San Andreas or Haiyuan Faults.

2. The implication of intense seismicity at the Gulang seismic zone

Another region (region 3 in Figure 3) with intense background seismicity and repeating earthquakes is located near the epicenter of the 1927 Gulang earthquake, north of the HYF (Figure 6). Yang (2017) performed repeating earthquake detections in this region, and found similar patterns of repeating clusters. While there are no

328 corresponding faults mapped on the surface, relocated seismicity is concentrated
329 along two linear zones trending NNW to nearly NS, indicating two possible hidden
330 faults at depth (Figure 6). Such interpretation is consistent with the available focal
331 mechanisms of moderate-size events in this region, which are predominately
332 NNW-SEE trending right-lateral strike slip events.

333 Wang (2018) named the intensive seismic activity in this region as “Gulang
334 seismic window”, which are stress sensitive regions in the aftershock zones following
335 large earthquakes. Because this region is spatially close to the rupture zone of the
336 1927 M~8 Gulang earthquake, it is possible that they are extended aftershocks of the
337 Gulang earthquake. This interpretation is consistent with general observations of
338 long-tailed aftershock activity, especially in intraplate regions around the world (Ebel
339 et al., 2000; Stein and Liu, 2009). Even at plate boundary regions, large earthquakes
340 can potentially affect the deformation pattern and cycles of small to moderate-size
341 earthquakes at nearby distances. For example, Ben-Zion et al. (1993) employed 3-D
342 finite-element modeling to infer that the M6-type Parkfield earthquakes are driven by
343 time-dependent loading from the 1857 M8 Fort Tejon earthquake. Hence, we argue
344 that intensive earthquake swarms and repeating earthquakes in this region are likely
345 driven by the relaxation process induced by the 1927 M~8 Gulang earthquake.

346 Based on seismic velocity inversions, Deng et al. (2018) found that this region is
347 mechanically weaker compared with the North China Craton in the north, and the
348 central Qilian in the south. This is comparable with the earthquake swarms at Belo

Jardim, NE Brazil (Lopes et al., 2010), and the Salton Trough South California (Lohman and McGuire, 2007), which are likely occurred at the pre-existing weak zones.

Conclusions

Based on waveform cross-correlations and relocations, we systematically search for repeating earthquakes in NE Tibet with ten years of seismic data. The repeating earthquakes are found in certain regions. Laohushan section of HYF has several repeating earthquakes, whose epicenters are located to the west of the peak creep region indicated by InSAR observations. The slip rate estimated from the repeating earthquakes is slightly smaller than the geodetic and geological observation. However, our estimation is based on assumed constant stress drops and has several limitations, and hence could be considered as a lower bound for the slip rate. In addition, the relocated microearthquakes are mostly located deeper than 4 km, indicating the geodetically observed creep is constrained at shallow depth, while faults at deeper depth remain locked. Hence, we infer that these repeating earthquakes likely mark the boundary between the creep and locked region. We also find many repeating earthquakes following the 2016 M6.4 Menyuan mainshock. The intense seismicity at the Gulang seismic zone is aligned along two linear zones indicating two possible hidden faults. This region may be intrinsically weak and hence these repeating events can be driven by the long-term relaxation process of the 1927 Gulang earthquake. In

comparison, repeating events related to mining explosions in this region have different waveforms from natural earthquakes, and can be readily identified based on several diagnostic features.

Acknowledgments

Waveform data for this study are provided by Data Management Centre of China National Seismic Network at Institute of Geophysics' China Earthquake Administration (doi:10.11998/SeisDmc/SN, http://www.seisdmc.ac.cn). We also thank Dr. Zhigang Yang and Dr. Yanyan Han at China Earthquake Networks Center (CENC), Dr. Xiaona Wang at Earthquake Administration of Guangdong Province, provides the catalog. Datasets for this research are included in its supplementary information files. This work was funded by the Strategic Priority Research Program (B) of the Chinese Academy of Sciences (grant XDB18000000), Youth Innovation Promotion Association CAS (YIPA) and Tuguangchi Award for Excellent Young Scholar (TGC201702).

References:

Abercrombie, R. E. (1996). The magnitude-frequency distribution of earthquakes recorded with deep seismometer at Cajon Pass, southern California. Tectonophysics, 261, 1-7, https://doi.org/10.1016/0040-1951(96)00052-2

Beeler, N.M., Lockner, D.L., & Hickman, S.H. (2001). A simple stick-slip and creep-slip model

for repeating earthquakes and its implication for microearthquakes at Parkfield. B Seismol Soc Am, 91, 1797-1804. https://doi.org/10.1785/0120000096

Ben-Zion, Y., Rice, J. R., & Dmowska, R. (1993). Interaction of the San Andreas Fault Creeping Segment with Adjacent great rupture zones and earthquake recurrence at Parkfield. Journal of Geophysical Research: Solid Earth, 98(B2), 2135-2144. https://doi.org/10.1029/92JB02154

Bisrat, S., DeShon, H.R., & Rowe, C. (2012). Microseismic swarm activity in the New Madrid seismic zone. Bull.Seismol. Soc. Am., 102, 1167-78. https://doi.org/10.1785/0120100315

Bürgmann, R., Schmidt, D., Nadeau, R.M., d’ Alessio, M., Fielding, E., et al. (2000). Earthquake potential along the Northern Hayward Fault, California. Science, 289, 1178-82. https://doi.org/10.1126/science.289.5482.1178

Chen, K.H., Nadeau, R.M., & Rau, R-J. (2007).Towards a universal rule on the recurrence interval scaling of repeating earthquakes? Geophys. Res. Lett., 34, L16308. https://doi.org/10.1029/2007GL030554

Chen, T., Liu-Zeng, J., Shao, Y.X., Zhang, P.Z, Oskin, M.E., Lei, Q.Y., & Li, Z.F. (2018). Geomorphic offsets along the creeping Laohu Shan section of the Haiyuan fault, northern Tibetan Plateau. Geosphere, 14, 3, 1165-1186. https://doi.org/10.1130 /GES01561.1.

Crotwell, H. P., Owens, T. J., & Ritsema, J. (1999). The TauP Toolkit: Flexible seismic travel-time and ray-path utilities, Seismological Research Letters, 70, 154–160. https://doi.org/10.1785/gssrl.70.2.154

Daout, S., Jolivet, R., Lasserre, C., Doin, M. P., Barbot, S., Tapponnier, P., et al. (2016). Along-strike variations of the partitioning of convergence across the Haiyuan fault system

415 detected by InSAR. Geophysical Journal International, 205(1), 536-547.
416 https://doi.org/10.1093/gji/ggw028
417 Deng, Y., Li, J., Song, X., & Zhu, L. (2018). Joint Inversion for Lithospheric Structures:
418 Implications for the Growth and Deformation in Northeastern Tibetan Plateau. Geophysical
419 Research Letters, 45(9), 3951-3958. https://doi.org/10.1029/2018GL077486
420 Gaudemer, Y., Tapponnier, P., Meyer, B., Peltzer, G., Shunmin, G., Zhitai, C., et al. (1995.)
421 Partitioning of crustal slip between linked, active faults in the eastern Qilian Shan, and
422 evidence for a major seismic gap, the 'Tianzhu gap', on the western Haiyuan Fault, Gansu
423 (China). Geophysical Journal International, 120, 599-645.
424 https://doi.org/10.1111/j.1365-246X.1995.tb01842.x
425 Cui, Z., Chen, Z., Wang, Q., & Li, J. (2019). Characteristics of focal mechanism and stress in the
426 North-South Seismic Belt of China. Earthquakes, 39, 1-10. (In Chinese with English abstract)
427 Harris, R.A. (2017). Large earthquakes and creeping faults. Rev. Geophys., 55, 169-198,
428 https://doi.org/10.1002/2016RG000539.
429 Igarashi, T., Matsuzawa, T., & Hasegawa, A. (2003). Repeating earthquakes and interplate
430 aseismic slip in the northeastern Japan subduction zone, J. Geophys. Res., 108, 2249.
431 https://doi.org/10.1029/2002JB001920
432 Jolivet, R., Lasserre, C., Doin, M.P., Guillaso, S., Peltzer, G., Dailu, R., et al. (2012). Shallow
433 creep on the Haiyuan fault (Gansu, China) revealed by SAR interferometry. Journal of
434 Geophysical Research, 117, B06401. http://dx.doi.org/10.1029/2011JB008732
435 Jolivet, R., Lasserre, C., Doin, M.P., Peltzer, G., Avouac, J.P., Sun, J., & Dailu, R. (2013).

436 Spatio-temporal evolution of aseismic slip along the Haiyuan fault, China: Implications for
437 fault frictional properties. Earth and Planetary Science Letters, 377, 23-33.
438 http://dx.doi.org/10.1016/j.epsl.2013.07.020
439 Kanamori, H., & Anderson, D.L. (1975), Theoretical basis for some empirical relations in
440 seismology, Bull. Seismol. Soc. Am., 65, 1073–1095.
441 Kaneko, Y., Fialko, Y., Sandwell, D. T., Tong, X., & Furuya, M. (2013), Interseismic deformation
442 and creep along the central section of the North Anatolian Fault (Turkey): InSAR
443 observations and implications for rate - and - state friction properties, J. Geophys. Res. Solid
444 Earth, 118, 316-331. http://dx.doi.org/10.1029/2012JB009661.
445 Karabacak, V., Altunel, E., & Cakir, Z. (2011). Monitoring aseismic surface creep along the North
446 Anatolian Fault (Turkey) using ground-based LIDAR. Earth and Planetary Science Letters,
447 304(1), 64-70. https://doi.org/10.1016/j.epsl.2011.01.017
448 Lengliné, O., & Marsan, D. (2009), Inferring the coseismic and postseismic stress changes caused
449 by the 2004 Mw = 6 Parkfield earthquake from variations of recurrence times of
450 microearthquakes. J. Geophys. Res., 114, B10303. http://dx.doi.org/10.1029/2008JB006118.
451 Lopes, A. E. V., Assumpção, M., Do Nascimento, A. F., Ferreira, J. M., Menezes, E. A. S., &
452 Barbosa, J. R. (2010). Intraplate earthquake swarm in Belo Jardim, NE Brazil: reactivation of
453 a major Neoproterozoic shear zone (Pernambuco Lineament). Geophysical Journal
454 International, 180(3), 1303-1312. http://dx.doi.org/10.1111/j.1365-246X.2009.04485.x
455 Lasserre, C., Bukchin, B., Bernard, P., Tapponnier, P., Gaudemer, Y.,Mostinsky, A. & Dailu, R.
456 (2001). Source parameters and tectonic origin of the 1996 June 1 Tianzhu (Mw = 5.2) and

1995 July Yongden (Mw = 5.6) earthquakes near the Haiyuan fault (Gansu, China). Geophys. J. Int., 144, 206–220. https://doi.org/10.1046/j.1365-246x.2001.00313.x

Lasserre, C., Gaudemer, Y., Tapponnier, P., Mériaux, A.S., Van der Woerd, J., Daoyang, Y., et al. (2002). Fast late Pleistocene slip rate on the Leng Long Ling segment of the Haiyuan fault, Qinghai, China. J. Geophys. Res., 107(B11), 2276. https://doi.org/10.1029/2000JB000060

Li, C., Zhang, P.-Z., Yin, J., & Min, W. (2009). Late Quaternary left-lateral slip rate of the Haiyuan fault, northeastern margin of the Tibetan Plateau. Tectonics 28, TC5010. https://doi.org/10.1029/2008TC002302

Li, L., Chen, Q-F., Cheng, X., & Niu, F. (2007). Spatial clustering and repeating of seismic events observed along the 1976 Tangshan fault, north China. Geophys. Res. Lett. 34, L23309. https://doi.org/10.1029/2007GL031594

Li, L., Chen, Q., Niu, F., & Su, J. (2011), Deep slip rates along the Longmen Shan fault zone estimated from repeating microearthquakes. J. Geophys. Res., 116, B09310. https://doi.org/10.1029/2011JB008406

Li, Y., Gan, W., Wang, Y., Chen, W., Liang, S., Zhang, K., & Zhang, Y. (2016). Seismogenic structure of the 2016 Ms6.4 Menyuan earthquake and its effect on the Tianzhu seismic gap. Geodesy and Geodynamics 7, 230-236. https://doi.org/10.1016/j.geog.2016.07.002

Liu, J., Ren, Z., Zhang, H., Li, C., Zhang, Z., Zheng, W., et al. (2018). Late Quaternary slip rate of the Laohushan Fault within the Haiyuan fault zone and its tectonic implications. Chinese Journal of Geophysics 61, 1281-1297. https://doi.org/10.6038/cjg2018L0364.

Liu, M., Li, H., Peng, Z., Ouyang, L., Ma, Y., Ma, J., et al. (2019). Spatial-temporal distribution of

early aftershocks following the 2016 Ms 6.4 Menyuan, Qinghai, China Earthquake. Tectonophysics 766, 469-479. https://doi.org/10.1016/j.tecto.2019.06.022

Liu-Zeng, J., Klinger, Y., Xu, X., Lasserre, C., Chen, G., Chen, W., et al. (2007). Millennial recurrence of large earthquakes on the Haiyuan fault near Songshan, Gansu Province, China. Bulletin of the Seismological Society of America, 97, 1B, 14-34. https://doi.org/10.1785/0120050118

Liu-Zeng, J., Chen, T., Zhang, P.Z., Zhang, H.P., Zheng, W.J., Ren, Z.K., et al. (2013). Illuminating the active Haiyuan fault, China by Airborne Light Detection and Ranging. Chinese Science Bulletin, 58, 41-45. http://dx.doi.org/10.1360/972012-1526

Lohman, R. B., & McGuire, J. J. (2007). Earthquake swarms driven by aseismic creep in the Salton Trough, California. Journal of Geophysical Research: Solid Earth, 112(B4). http://dx.doi.org/10.1029/2006jb004596

Nadeau, R.M., Foxall, W., & McEvilly, T.V. (1995). Clustering and periodic recurrence of microearthquakes on the San Andreas fault at Parkfield, California. Science 267, 503–507. http://dx.doi.org/10.1126/science.267.5197.503

Nadeau, R.M., & McEvilly, T.V., (1999). Fault slip rates at depth from recurrence intervals of repeating mi-croearthquakes. Science 285, 718-21. http://dx.doi.org/10.1126/science.285.5428.718

Nadeau, R.M., & McEvilly, T.V. (2004). Periodic pulsing of characteristic microearthquakes on the San Andreas Fault. Science, 303, 220-22. http://dx.doi.org/10.1126/science.1090353

Noda, H., & Lapusta, N. (2013) Stable creeping fault segments can become destructive as a result

499 of dynamic weakening. Nature, 493, 518–521. http://dx.doi.org/10.1038/nature11703.

500 Niu, F., Silver, P.G., Nadeau, R.M., & McEvilly, T.V. (2003). Migration of seismic scatterers
501 associated with the 1993 Parkfield aseismic transient event. Nature, 426, 544-48.
502 http://dx.doi.org/ 10.1038/nature02151

503 Ozener, H., Arpat, E., Ergintav, S., Dogru, A., Cakmak, R., Turgut, B., & Dogan, U. (2010),
504 Kinematics of the eastern part of the North Anatolian Fault Zone. J. Geodyn., 49(3–4), 141–
505 150. http://dx.doi.org/10.1016/j.jog.2010.01.003.

506 Peng, Z., & Ben-Zion, Y. (2005), Spatio-temporal variations of crustal anisotropy from similar
507 events in aftershocks of the 1999 M7.4 İzmit and M7.1 Duzce, Turkey, earthquake
508 sequences. Geophys. J. Int., 160, 1027-1043.
509 https://doi.org/10.1111/j.1365-246X.2005.02569.x

510 Peng, Z., & Ben-Zion, Y. (2006), Temporal changes of shallow seismic velocity around the
511 Karadere-Duzce branch of the north Anatolian fault and strong ground motion. Pure Appl.
512 Geophys., 163, 567-599. http://dx.doi.org/10.1007/s00024-005-0034-6.

513 Press, W., Flannery, B., Teukolsk, S., & Vetterling, W. (1986). Numerical Recipes. In: Cambridge
514 Univ. Press, Cambridge.

515 Poupinet, G., Ellsworth, W.L., & Frechet, J. (1984). Monitoring velocity variations in the crust
516 using earthquake doublets: an application to the Calaveras fault, California. J Geophys. Res.,
517 89, 5719–5731. https://doi.org/10.1029/JB089iB07p05719

518 Ruan, X., Meng, X., Peng, Z., Long, F., & Xie, R. 2017. Microseismic activity in the last 5
519 months before the Mw7.9 Wenchuan earthquake. Bull. Seismol. Soc. Am., 107(4),

1582-1592. https://doi.org/doi:10.1785/0120160032.

Rubin, A.M. (2002). Using Repeating Earthquakes to Correct High-Precision Earthquake Catalogs for Time-Dependent Station Delays. Bulletin of the Seismological Society of America, 92(5), 1647–1659. https://doi.org/10.1785/0120010180

Rubinstein, J.L., & Beroza, G.C. (2004). Evidence for Widespread Nonlinear Strong Ground Motion in the MW 6.9 Loma Prieta Earthquake. Bulletin of the Seismological Society of America, 94 (5), 1595–1608. https://doi.org/10.1785/012004009

Shirzaei, M., R. & Bürgmann, Taira, T. (2013), Implications of recent asperity failures and aseismic creep for time-dependent earthquake hazard on the Hayward Fault, Earth Planet. Sci. Lett., 371–372, 59–66. https://doi.org/10.1016/j.epsl.2013.04.024

Schaff, D.P., & Beroza, G.C. (2004). Coseismic and postseismic velocity changes measured by repeating earthquakes. J. Geophys. Res., 109, B10302. https://doi.org/10.1029/2004JB003011

Schaff, D. P., & Richards, P. G. (2004). Repeating Seismic Events in China. Science, 303(5661), 1176. http://dx.doi.org/10.1126/science.1093422

Schmidt, D. A., Bürgmann, R., Nadeau, R. M., & d'Alessio, M. (2005), Distribution of aseismic slip rate on the Hayward fault inferred from seismic and geodetic data. J. Geophys. Res., 110, B08406. http://dx.doi.org/10.1029/2004JB003397.

Simpson, R. W., J. J. Lienkaemper, & Galehouse, J.S. (2001), Variations in creep rate along the Hayward fault, California, interpreted as changes in depth of creep. Geophys. Res. Lett., 28, 2269–2272. https://doi.org/10.1029/2001GL012979.

Stein, S., & Liu, M. (2009). Long aftershock sequences within continents and implications for earthquake hazard assessment. Nature, 462(7269), 87-89. http://dx.doi.org/10.1038/nature08502

Stump, B. W., Hedlin, M. A. H., Pearson, D. C., & Hsu, V. (2002). Characterization of mining explosions at regional distances: Implications with the International Monitoring System, Rev. Geophys., 40 (4), 1011. https://doi.org/10.1029/1998RG000048

Taira, T., Silver, P.G., Niu, F., & Nadeau, R.M. (2009). Remote triggering of fault - strength changes on the San Andreas Fault at Parkfield. Nature, 461(7264), 636–639. https://doi.org/10.1038/nature08395

Trugman, D.T., & Shearer, P.M. (2017). GrowClust: A Hierarchical Clustering Algorithm for Relative Earthquake Relocation, with Application to the Spanish Springs and Sheldon, Nevada, Earthquake Sequences. Seismological Research Letters 88, 379-391. https://doi.org/10.1785/0220160188

Uchida, N., Matsuzawa, T., Igarashi, T., & Hasegawa, A. (2003). Interplate quasi-static slip off Sanriku, NE Japan, estimated from repeating earthquakes. Geophys. Res. Lett., 30, 1801, http://dx.doi.org/10.1029/2003GL017452, 15.

Uchida, N. (2019). Detection of repeating earthquakes and their application in characterizing slow fault slip. Progress in Earth and Planetary Science 6, 40. https://doi.org/10.1186/s40645-019-0284-z

Uchida, N., & Bürgmann, R. (2019). Repeating earthquakes. Annual Review of Earth and Planetary Sciences, 47, 305–332. https://doi.org/10.1146/annurev-earth-053018-060119

562 Vidale, J.E., ElIsworth, W.L., Cole, A., & Marone, C. (1994). Variations in rupture process with
563 recurrence interval in a repeated small earthquake. Nature, 368, 624-626.
564 https://doi.org/10.1038/368624a0
565 Wang, L.X. (2018). Focal Mechanism of Small and Medium Earthquakes and Its Dynamic
566 Significance in Gansu “Gulang Window”. Master thesis. Lanzhou Institute of Seismology.
567 Wang, W.-T., Zhang, P.-Z., Kirby, E., Wang, L.-H., Zhang, G.-L., Zheng, D.-W., et al. (2011). A
568 revised chronology for Tertiary sedimentation in the Sikouzi basin: Implications for the
569 tectonic evolution of the northeastern corner of the Tibetan Plateau. Tectonophysics, 505,
570 100-114. https://doi.org/10.1016/j.tecto.2011.04.006
571 Yang, P. (2017). Deep Slip Rates Along the Active Faults in Gulang Region Estimated from
572 Repeating Microearthquakes. Master thesis. Lanzhou Institute of Seismology.
573 Yao, D., Walter, J.I., Meng, X., Hobbs, T.E., Peng, Z., Newman, A.V., et al. (2017). Detailed
574 spatiotemporal evolution of microseismicity and repeating earthquakes following the 2012
575 mw 7.6 Nicoya earthquake. J. Geophys. Res., 122, 524–542.
576 https://doi.org/10.1002/2016JB013632
577 Yao, W., Liu-Zeng, J., Oskin, M.E., Wang, W., Li, Z., Prush, V., et al. (2019). Reevaluation of the
578 Late Pleistocene slip rate of the Haiyuan fault near Songshan, Gansu province, China. Journal
579 of Geophysical Research: Solid Earth, 124. https://doi.org/10.1029/2018JB016907
580 Yu, W.C. (2013). Shallow-focus repeating earthquakes in the Tonga–Kermadec–Vanuatu
581 subduction zones. B Seismol Soc Am 103, 463–486. https://doi.org/10.1785/0120120123
582 Zhang, P., Molnar, P., Zhang, W., Deng, Q., Wang, Y., Burchfiel, B.C., et al. (1988). Bounds on the

583 Average Recurrence Interval of Major Earthquakes Along the Haiyuan Fault In North-Central
584 China. Seismological Research Letters, 59, 81-89. https://doi.org/10.1785/gssrl.59.3.81
585 Zheng, W., Zhang, P., He, W., Yuan, D., Shao, Y., Zheng, D., et al. (2013), Transformation of
586 displacement between strike-slip and crustal shortening in the northern margin of the Tibetan
587 Plateau: Evidence from decadal GPS measurements and late Quaternary slip rates on faults.
588 Tectonophysics, 584, 267–280. https://doi.org/10.1016/j.tecto.2012.01.006
589 Zheng, G., Wang, H., Wright, T. J., Lou, Y., Zhang, R., Zhang, W., et al. (2017). Crustal
590 deformation in the India-Eurasia collision zone from 25 years of GPS measurements. Journal
591 of Geophysical Research: Solid
592 Earth, 122, 9290– 9312. https://doi.org/10.1002/2017JB014465
593 Zheng, X.-F., Yao, Z.-X., Liang, J.-H., & Zheng, J. (2010). The role played and opportunities
594 provided by IGP DMC of China National Seismic Network in Wenchuan earthquake disaster
595 relief and researches. Bull. Seism. Soc. Am., 100, 2866-2872.
596 https://doi.org/10.1785/0120090257
597

598 Figure Caption

599 Figure 1. (a) The geological setting, major faults (pink), microearthquakes (black dots) and station
600 distribution (blue triangles) in NE Tibet. The inset marks the study region in a larger map of Tibet.
601 (b) The focal mechanism of M>3.5 events and GPS velocity in this region. The focal mechanisms
602 are obtained from Cui et al., (2019) and GCMT catalog. HYF: Haiyuan fault; XHF: Xianshuihe
603 fault. The GPS data is sourced from Zheng et al., 2017, JGR. The fault geometry is obtained from

604 Taylor and Yin (2009).

605

606 Figure 2. Distributions of clusters of repeating earthquake in NE Tibet. Events with white colors
607 are background seismicity, and cluster with different numbers in each family is marked with
608 different colors. The detailed information of marked faults is shown in Figure 1. 8 sub-regions are
609 marked for subsequent analysis.

610

611 Figure 3. (a) A map view showing the repeating earthquakes along the Laohushan section of the
612 HYF. The M≥4 events are noted in the figure. The red color indicates the cluster with at least 8
613 events. The blue box indicates the possible creep region (Jolivet et al., 2012). The black box marks
614 the region for calculating the slip rate. The black square indicates the start point (0 km) on (b-c).
615 (b) Along-strike distribution of the average, horizontal fault parallel, creep rate measured on
616 average velocity fields determined by Jolivet et al. (2013). (c) Along-strike distance versus time
617 for both background events and repeating clusters. The radius of circle corresponds to the
618 magnitude/rupture size. The fault geometry comes from the airborne LiDAR (Liu-Zeng et al.,
619 2013). The focal mechanisms are obtained from Cui et al., (2019) and GCMT catalog.

620

621 Figure 4. The vertical component waveforms recorded at station GS.YDT for a single cluster with
622 8 members.

623

624 Figure 5. (a) The map distribution of repeating earthquakes and background events around the
625 aftershock zone of the 2016 M6.4 Mengyuan mainshock. (b) The time distribution of repeating

626 earthquakes and background events at Menyuan. The M≥4 events are noted in the figure. The fault
627 geometry is from Liu et al. (2019). The blue color indicates the cluster with at least 4 events. The
628 focal mechanisms are obtained from GCMT catalog.
629
630 Figure 6. (a) The map distribution of repeating earthquakes and background events at the Gulang
631 seismic zone. (b) The time distribution of repeating earthquakes and background events at the
632 Gulang seismic zone. The M≥4 events are noted in the figure. The red color indicates the cluster
633 has at least 8 events. The red arrows (C1, C2, C3, C4) indicate the possible triggered swarms. (c)
634 The relocated background events (including repeaters) at the Gulang seismic zone. The events
635 distribution before and after relocation within the shading region marked in (a) and (c).
636
637 Figure 7. The histogram of the event time with local time zone at four regions with likely mining
638 activities.
639
640 Figure 8. The local topography is shown in Google Map at four regions with likely mining
641 activities.
642
643 Figure 9. The vertical component waveforms recorded at stations in four regions with clusters
644 more than 8 events.
645
646 Figure 10. The events (a) and repeaters (b) before and after relocation along and across strike in
647 the Laohushan section of the HYF. The events located in the box are marked in Fig. 4. 0 km for

the along strike is the left boundary of the black box at HYF. The shading region indicates the possible creep region. The black dashed lines mark the changes before and after relocation.

Figure1.

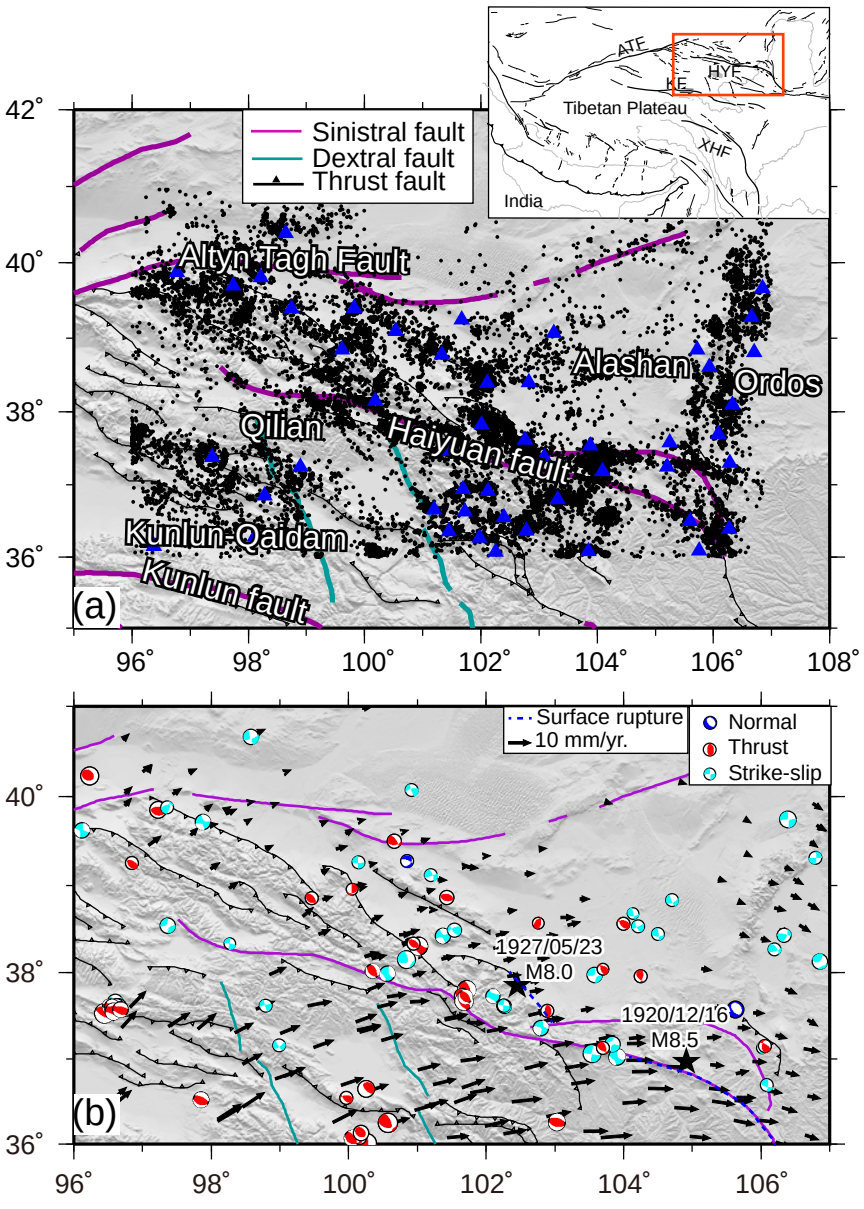
Sinistral fault
Dextral fault
Thrust fault
Altyn Tagh Fault
Alashan
Ordos
Qilian
Haiyuan fault
Kunlun-Qaidam
Kunlun fault
(a)
ATF
KF
HYF
XHF
Tibetan Plateau
India
42˚
40˚
38˚
36˚
96˚
98˚
100˚
102˚
104˚
106˚
108˚
Surface rupture
10 mm/yr.
Normal
Thrust
Strike-slip
1927/05/23
M8.0
1920/12/16
M8.5
(b)

Figure2.

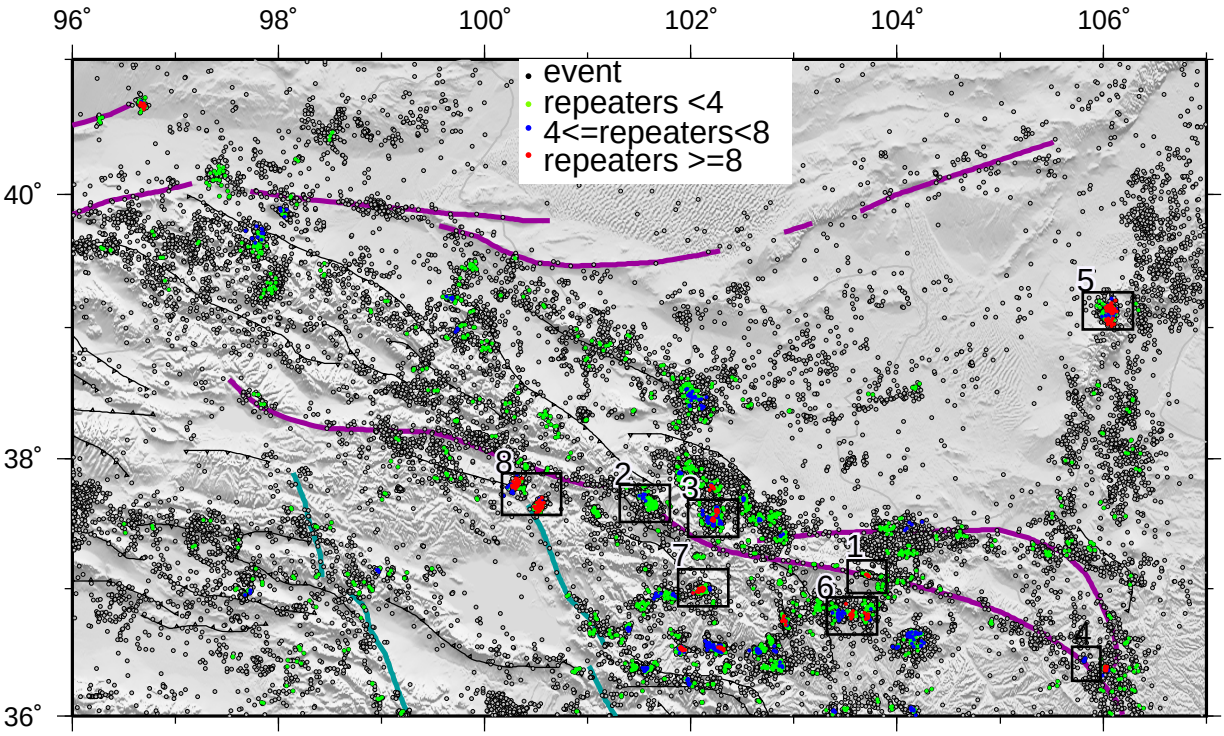
96˚
98˚
100˚
102˚
104˚
106˚
40˚
38˚
36˚
event
repeaters <4
4<=repeaters<8
repeaters >=8
1
2
3
4
5
6
7
8

Figure3.

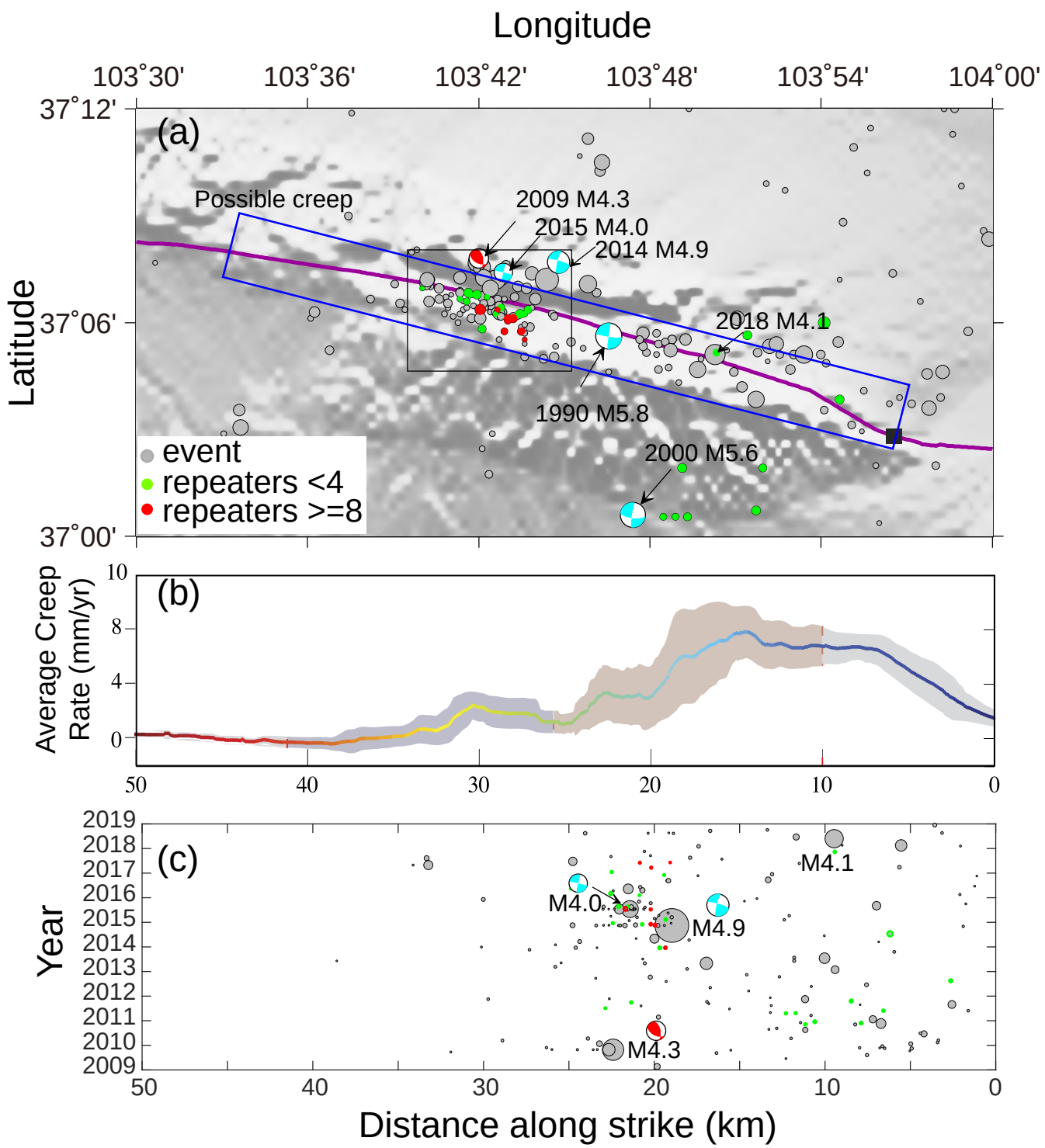
Longitude
103˚30'
103˚36'
103˚42'
103˚48'
103˚54'
104˚00'
37˚12'
37˚06'
37˚00'
Latitude
(a)
Possible creep
2009 M4.3
2015 M4.0
2014 M4.9
2018 M4.1
1990 M5.8
2000 M5.6
event
repeaters <4
repeaters >=8
(b)
Average Creep Rate (mm/yr)
10
8
4
0
50
40
30
20
10
0
(c)
Year
2019
2018
2017
2016
2015
2014
2013
2012
2011
2010
2009
M4.1
M4.0
M4.9
M4.3
50
40
30
20
10
0
Distance along strike (km)

Figure4.

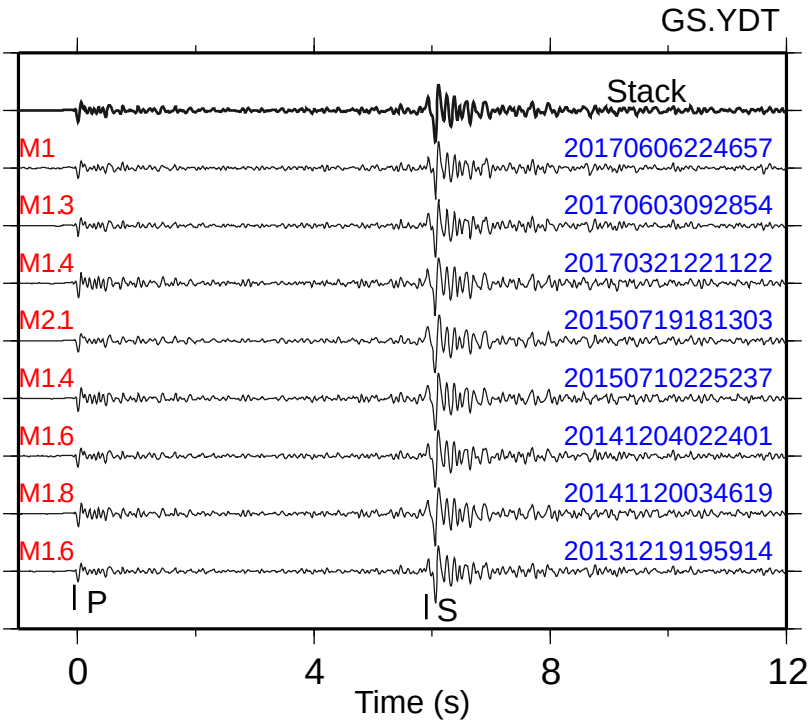
GS.YDT
Stack
M1
20170606224657
M1.3
20170603092854
M1.4
20170321221122
M2.1
20150719181303
M1.4
20150710225237
M1.6
20141204022401
M1.8
20141120034619
M1.6
20131219195914
P
S
0
4
8
12
Time (s)

Figure5.

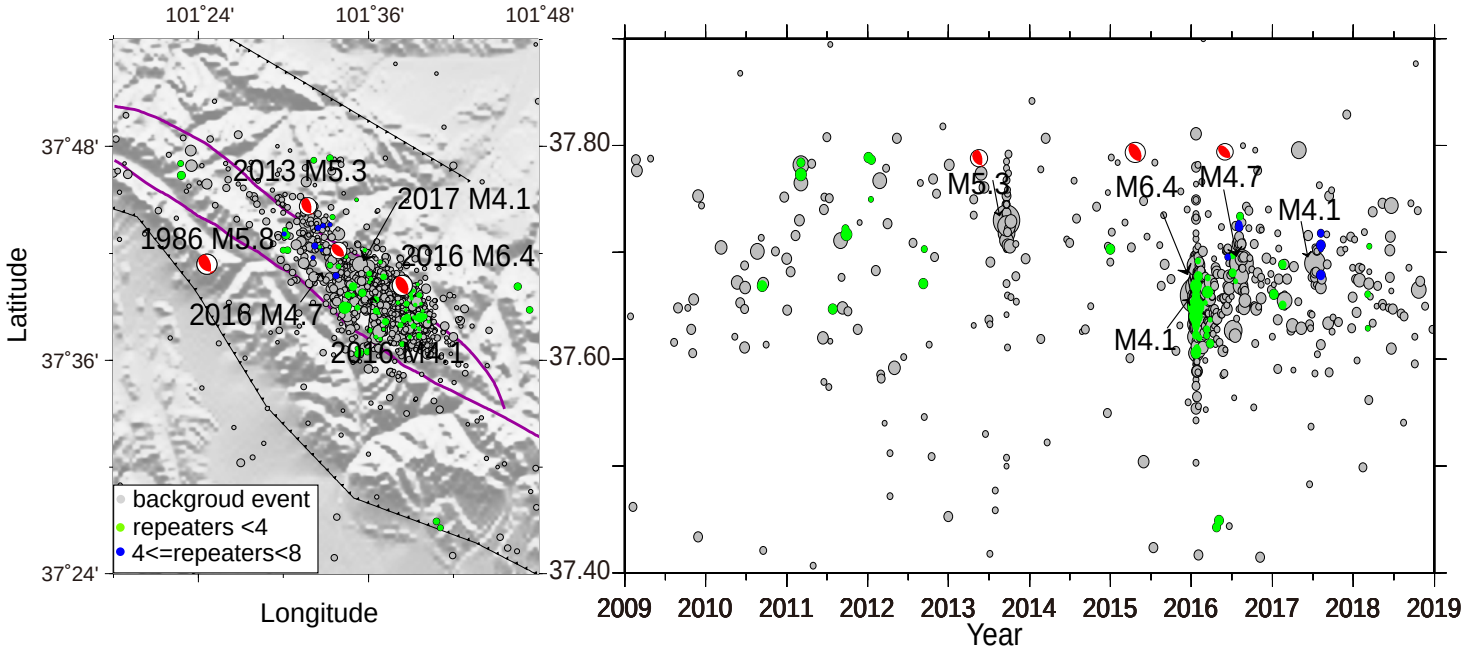
101˚24'
101˚36'
101˚48'
37˚48'
37˚36'
37˚24'
Latitude
Longitude
2013 M5.3
2017 M4.1
1986 M5.8
2016 M6.4
2016 M4.7
2016 M4.1
backgroud event
repeaters <4
4<=repeaters<8
37.80
37.60
37.40
M5.3
M6.4
M4.7
M4.1
M4.1
2009
2010
2011
2012
2013
2014
2015
2016
2017
2018
2019
Year

Figure6.

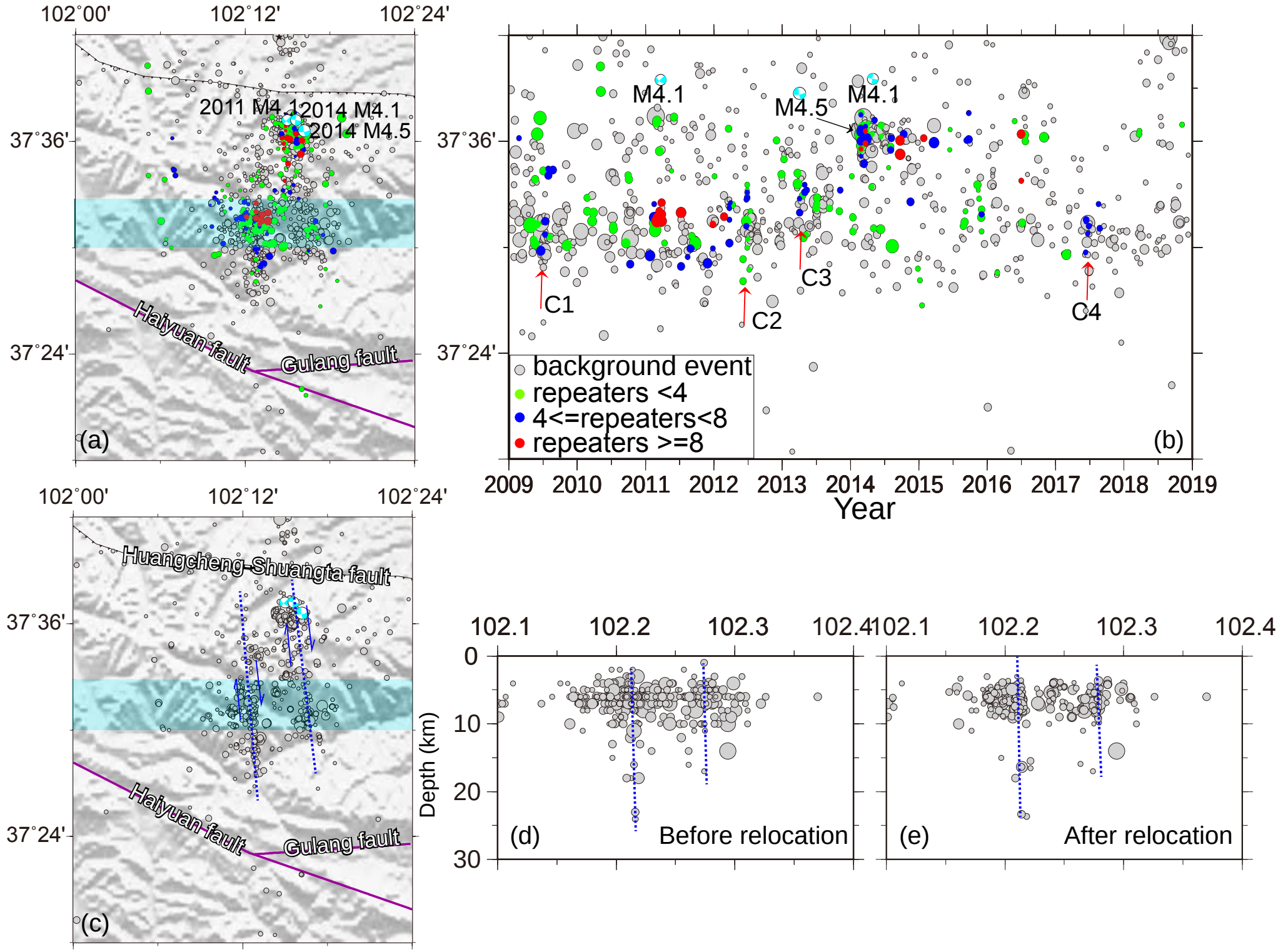
102˚00'
102˚12'
102˚24'
37˚36'
37˚24'
2011 M4.1
2014 M4.1
2014 M4.5
Haiyuan fault
Gulang fault
(a)
M4.1
M4.5
M4.1
C1
C2
C3
C4
background event
repeaters <4
4<=repeaters<8
repeaters >=8
(b)
2009
2010
2011
2012
2013
2014
2015
2016
2017
2018
2019
Year
Huangcheng-Shuangta fault
(c)
102.1
102.2
102.3
102.4
Depth (km)
0
10
20
30
(d)
Before relocation
(e)
After relocation

Figure7.

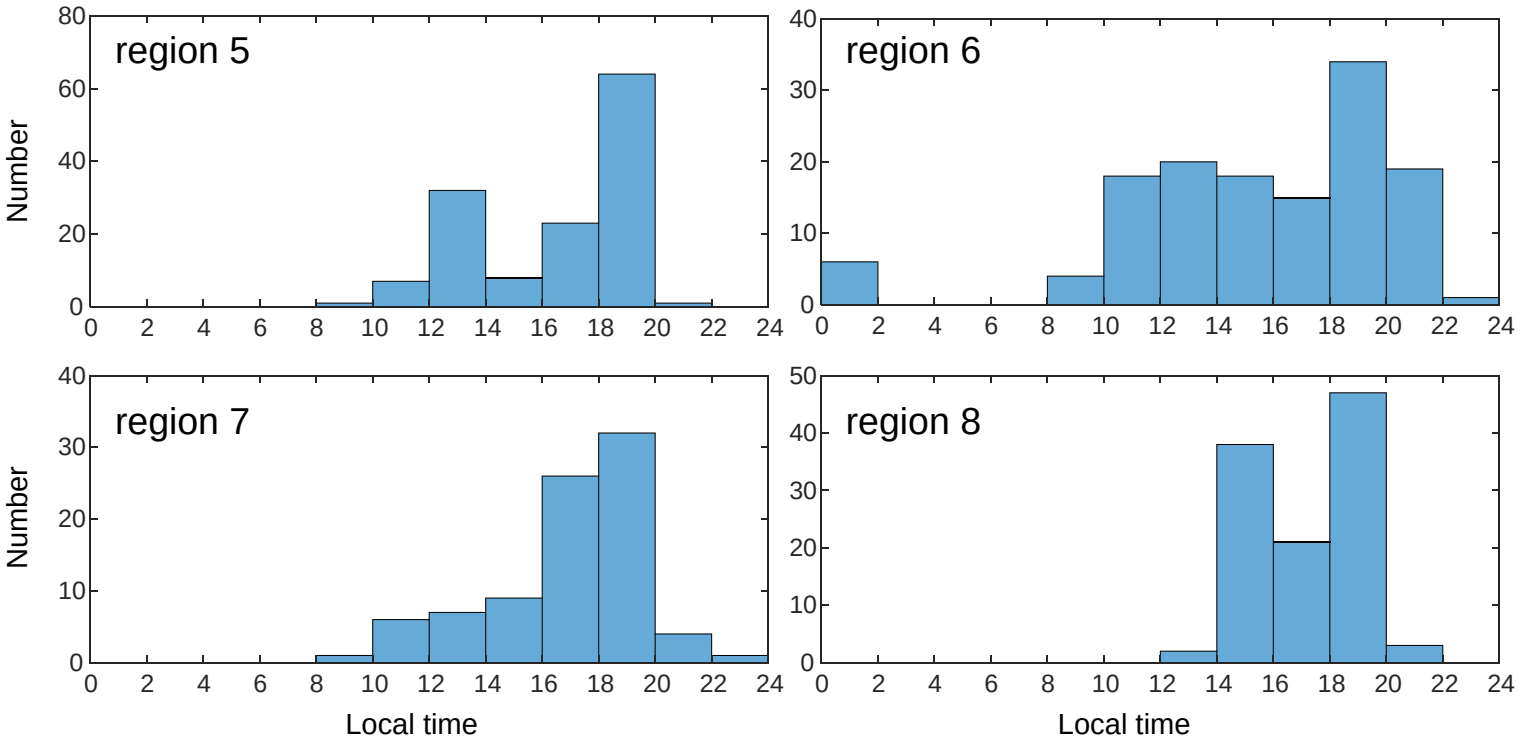
region 5
region 6
region 7
region 8
Number
Number
Local time
Local time

Figure8.


region 5
Google


region 6
Google


region 7
Google


region 8
S204
Google

Figure9.

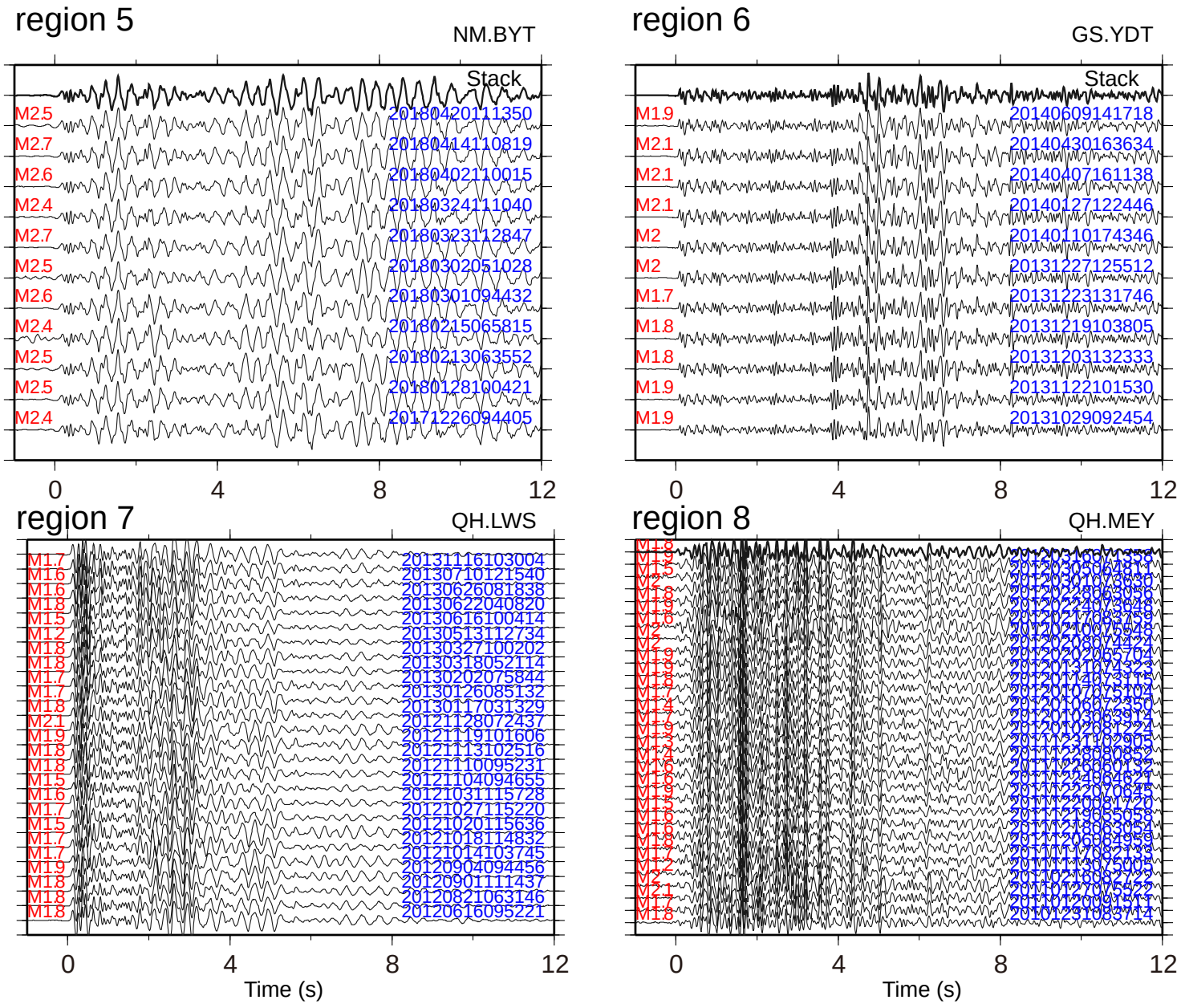
region 5
NM.BYT
Stack
M2.5 20180420111350
M2.7 20180414110819
M2.6 20180402110015
M2.4 20180324111040
M2.7 20180323112847
M2.5 20180302051028
M2.6 20180301094432
M2.4 20180215065815
M2.5 20180213063552
M2.5 20180128100421
M2.4 20171226094405
0 4 8 12
region 6
GS.YDT
Stack
M1.9 20140609141718
M2.1 20140430163634
M2.1 20140407161138
M2.1 20140127122446
M2 20140110174346
M2 20131227125512
M1.7 20131223131746
M1.8 20131219103805
M1.8 20131203132333
M1.9 20131122101530
M1.9 20131029092454
0 4 8 12
region 7
QH.LWS
M1.7 20131116103004
M1.6 20130710121540
M1.6 20130626081838
M1.8 20130622040820
M1.5 20130616100414
M1.2 20130513112734
M1.8 20130327100202
M1.8 20130318052114
M1.7 20130202075844
M1.7 20130126085132
M1.8 20130117031329
M2.1 20121128072437
M1.9 20121119101606
M1.8 20121113102516
M1.8 20121110095231
M1.5 20121104094655
M1.6 20121031115728
M1.7 20121027115220
M1.5 20121020115636
M1.7 20121018114832
M1.7 20121014103745
M1.9 20120904094456
M1.8 20120901111437
M1.8 20120821063146
M1.8 20120616095221
0 4 8 12
Time (s)
region 8
QH.MEY
0 4 8 12
Time (s)

Figure10.

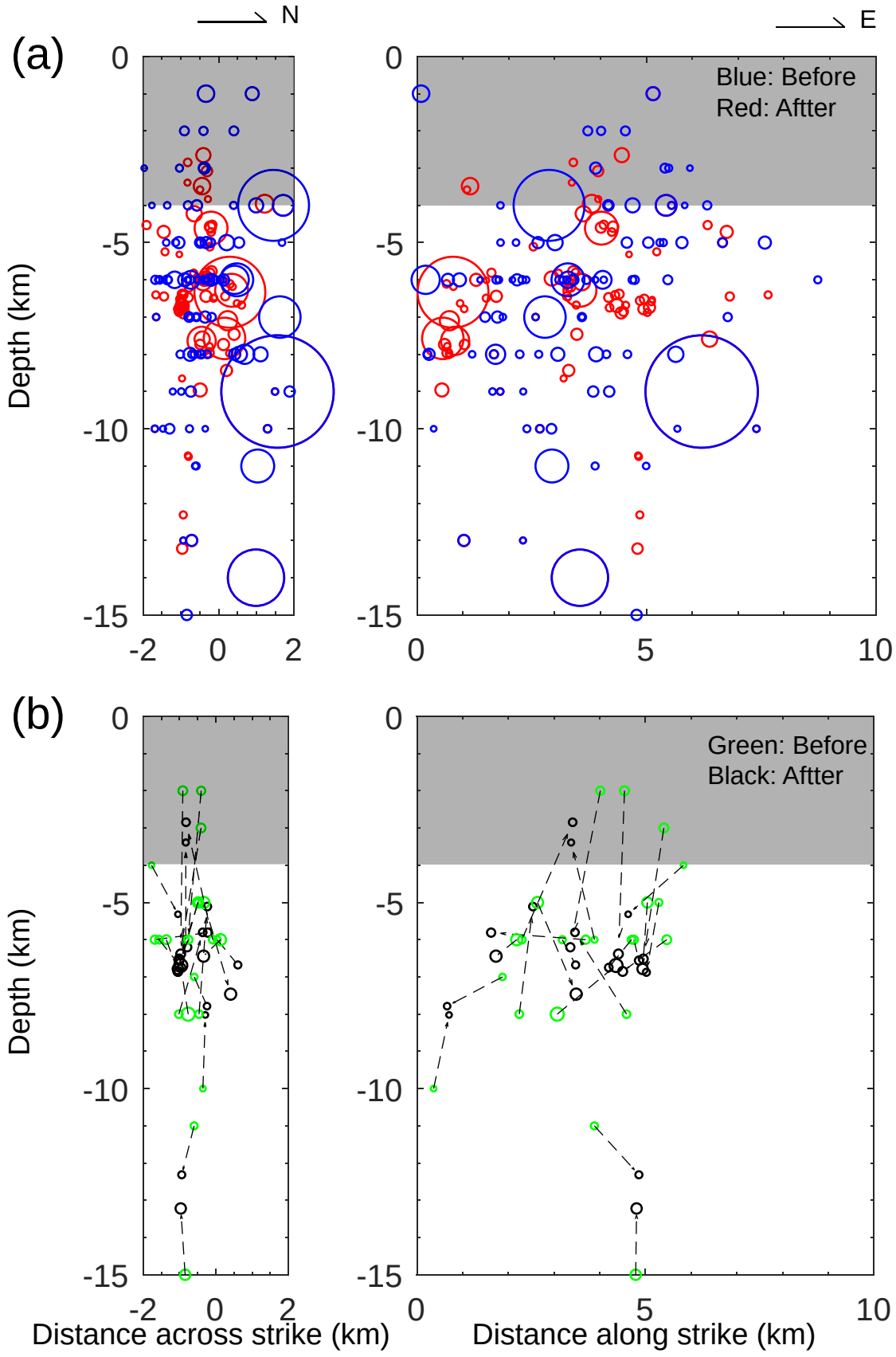
(a)
N
E
Blue: Before
Red: Aftter
Depth (km)
0
-5
-10
-15
-2
0
2
0
5
10
(b)
Green: Before
Black: Aftter
Depth (km)
Distance across strike (km)
Distance along strike (km)